THE JOURNAL OF PHYSICAL CHEMISTRY A

Article

pubs.acs.org/JPCA

# Dehydrohalogenation and Dehydration Reactions of *i*-$C_3H_7Br$ and *i*-$C_3H_7OH$ by Sodium Ions Studied by Guided Ion Beam Techniques and Quantum Chemical Methods

E. López,[§] J. M. Lucas,[§] J. de Andrés,[§] M. Albertí,[§] J. M. Bofill,[‡] and A. Aguilar*[,§]

[§]Departament de Química Física and [‡]Departament de Química Orgànica, Institut de Química Teòrica i Computacional, Universitat de Barcelona, Martí i Franquès, 1, 08028 Barcelona, Spain

**ABSTRACT:** Dehydrohalogenation and dehydration reactions of gas-phase *i*-$C_3H_7Br$ and *i*-$C_3H_7OH$ molecules induced by collision with $Na^+$, all participants being in their electronic ground state, were studied experimentally in our laboratory using a radiofrequency-guided ion beam apparatus and covering the 0.10−10.00 eV center of mass (CM) energy range. In $Na^+$ + *i*-$C_3H_7Br$ collisions the formation of $[C_3H_6–Na]^+$ and $[HBr–Na]^+$ by dehydrohalogenation was observed and quantified, as well as that of the ion−molecule adduct $[Na–i\text{-}C_3H_7Br]^+$ together with its decomposition products $C_3H_7^+$ and NaBr. In $Na^+$ + *i*-$C_3H_7OH$ collisions the dehydration product $[H_2O–Na]^+$ was also found, while $[C_3H_6–Na]^+$ was hardly detected. Moreover, the $[Na–i\text{-}C_3H_7OH]^+$ adduct formation as well as its decomposition into $C_3H_7^+$ and NaOH were also quantified. For all these processes, absolute reaction cross sections were measured as a function of the CM collision energy. From measured excitation functions, rate constants for the formation of $[C_3H_6–Na]^+$, $[HBr–Na]^+$, and $[H_2O–Na]^+$ at 303 K were obtained. Complementing the experiments, exhaustive ab initio structure calculations at the MP2 level of theory were performed, giving information on the most relevant features of the potential energy surfaces (PESs) where the dehydrohalogenation, dehydration, and decomposition reactions take place adiabatically for both collision systems. On these PESs different stationary points associated with potential energy minima and transition state barriers were characterized, and their connectivity was ensured using the intrinsic-reaction-coordinate method. The main topology features of the ab initio calculated PESs allowed a qualitative interpretation of the experimental data also exposing the role of the sodium ion as a catalyst in elimination reactions.

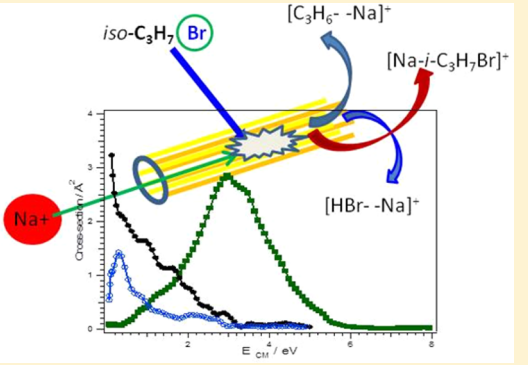


## 1. INTRODUCTION

The radio frequency guided ion beam (RF-GIB)[1] apparatus developed in our laboratory over the last 10 years was employed in studying the formation of adducts between alkali ions and polar molecules such as butanone and cyclohexanone[2] or nonpolar molecules like benzene[3] in the few electronvolt collision energy range. Taking into account that the study of ion−molecule reactions is of interest in such physical chemistry or chemical physics areas as atmospheric chemistry,[4,5] biological systems,[6] planetary atmospheres, and interstellar media[7] and that our experimental apparatus is suitable for generating alkali ions at low collision energies, we recently studied reactive processes in alkali ions colliding with some halogenated organic compounds and alcohols. In the middle and second half of the 1970s, Wieting[8] et al. as well as Allison and Ridge[9,10] observed the dehydrohalogenation (or dehydration) reactions of the corresponding halogenated compounds (or alcohols) induced by alkali ion collisions. The reactivity of the different ion−molecule systems strongly depended on the particular halogenated compound or alcohol as well as on the particular alkali ion, lithium being the most reactive one. Creasy and Farrar studied, among other systems, the dehydration of *tert*-butanol[11] as well as the dehydrohalogenations[12] of iso- and *n*-propyl chloride and isopropyl bromide induced by lithium ion collisions at low energy using molecular beam techniques and at a few defined collision energies, measuring the corresponding branching ratios for the different reaction channels. In our previous studies on ion−molecule dehydrohalogenation or dehydration reactions,[6,13−17] we measured the corresponding excitation functions for different reaction channels including some not previously observed.[9−12] These studies were complemented by ab initio calculations of the corresponding ground singlet state potential energy surfaces (PES) on which the reactive processes take place adiabatically at low collision energies.

In the present work we report on the reactive processes taking place in collisions between $Na^+$ and *i*-$C_3H_7Br$ or *i*-$C_3H_7OH$ molecules, all reactants being in their singlet ground state. According to previous experiments, we expected to

**Special Issue:** Piergiorgio Casavecchia and Antonio Lagana Festschrift

**Received:** December 4, 2015
**Revised:** January 8, 2016





DOI: 10.1021/acs.jpca.5b11869
J. Phys. Chem. A XXXX, XXX, XXX−XXX

observe the reactive channels leading to dehydrohalogenation or dehydration, respectively.

$$Na^+ + i - C_3H_7R \rightarrow [C_3H_6 - Na]^+ + HR \quad (1)$$

$$Na^+ + i\text{-}C_3H_7R \rightarrow C_3H_6 + [HR - Na]^+ \quad (2)$$

where R stands for Br or OH and producing propene as well as the hydrogen halide (or water). The reactant sodium ion is attached to propene (reaction channel 1) or to the hydrogen halide/water (reaction channel 2). Moreover, the decomposition reaction

$$Na^+ + i\text{-}C_3H_7R \rightarrow C_3H_7^+ + NaR \quad (3)$$

can also be expected to take place in the low collision energy range studied (0.10−10.00 eV). At the higher limit of this range, $C_3H_7^+$decomposition

$$C_3H_7^+ \rightarrow C_2H_3^+ + CH_4 \quad (4)$$

was also observed experimentally. To the best of our knowledge neither reaction 3 nor 4 for the systems studied here have been described in the bibliography, while reactions 2 and 3 were not observed in earlier studies of these systems.[9,10]

After the Introduction, in Section 2 a brief description on the experimental setup is given, and the experimental results for $Na^+ + i\text{-}C_3H_7R$ (R = Br, OH) collisions are shown. In Section 3 the quantum chemistry calculations used to characterize the adiabatic PES on which reactive collisions evolve are exposed, followed by a detailed description of the PES' main topologic features and their related chemical structures. Finally a discussion and an interpretation of the experimental results in the light of the ab initio quantum chemistry calculations are given.

## 2. EXPERIMENTAL SECTION

**2.1. A Brief Description of the Radio Frequency Guided Ion Beam Experimental Setup.** The experimental RF-GIB developed in our laboratory has been extensively described elsewhere,[1] so only a brief outline is given here. In the present study a pure $Na^+(^1S_0)$ beam is selected by a mass quadrupole filter from the beam generated by thermoionic effect on a suitable device (HeatWave Laboratories) heated to ∼1200 K. Filtered ions are collimated and focused into an octopole ion guide containing the thermal target gas at low pressure. The octopole field both guides the primary ions and gathers the ion products in a $4\pi$ solid angle. Both parent and product ions are refocused and mass analyzed by a second mass quadrupole and detected by a secondary electron multiplier. Vapors of pure and dry $i\text{-}C_3H_7R$ compounds are introduced in the octopole scattering cell through a vacuum pipeline controlled by a fine-pitch needle valve. Under experimental conditions the background pressure is kept in the $1 \times 10^{-6}$ to $1 \times 10^{-7}$ mbar range, and the pressure in the gas cell is $\sim 1 \times 10^{-5}$ mbar, low enough to ensure single collision conditions. All systems and ancillary electronics are PC-controlled with a software developed in our group using LabVIEW (© National Instruments). Performing the $Na^+ + i\text{-}C_3H_7R$ collisions at a fixed laboratory frame (LF) energy, the intensity of the primary ($I_0$) and product ($I_i$) ions are measured. The LF energy of the sodium ions in the beam is determined using the so-called retarding potential analysis method,[1,18] the octopole ion guide acting as the retarding energy analyzer. This gives a nearly Gaussian[1,18] ion energy distribution with some uncertainty measured by its full width at half-maximum (fwhm). Assuming that target molecules are stationary, each collision energy in the LF can be associated with a fixed collision energy $E_0$ in the center of mass (CM) frame, which takes into account the uncertainty of the ion beam energy distribution. Considering also the Doppler broadening on the ion beam energy distribution due to the fact that target molecules are not stationary,[19−21] the reactive cross-section at the CM collision energy $E_0$ is given by

$$\sigma_{exp}(E_0) = \frac{I_i}{I_0 nl} \quad (5)$$

where $n$ and $l$ stand for the target gas density in the reaction cell and its effective path length, respectively. The $nl$ product has been characterized in a previous calibration experiment[3,17] by comparing our results with those described by Koizumi and Armentrout[22] so that measured cross sections can be given in absolute units with an uncertainty of ∼30%.In the present experiments fwhm for $Na^+$ was ∼0.40 eV.

**2.2. Experimental Reactive Excitation Function in $Na^+ + i\text{-}C_3H_7Br$ Collisions.** Before measuring excitation functions for the different reaction channels in $Na^+ + i\text{-}C_3H_7Br$ collisions, product ions were characterized by doing a mass scan at a few different collision energies in the 1 to 200 mass/charge unit range. For this system, signals were detected at 104 and 65 $m/z$ units as expected for reactions 1 and 2 and related to the formation of $[C_3H_6{-}Na]^+$ and $[HBr{-}Na]^+$products. Another signal found at $m/z$ of 146 units can be associated with the formation of the ion−molecule adduct $[Na{-}\ i\text{-}C_3H_7Br]^+$. Additionally, on increasing the collision energy the formation of both $C_3H_7^+$ (43 $m/z$ units) and $C_2H_3^+$ (27 $m/z$ units) was observed according to reactions 3 and 4.

The cross-section CM energy dependences for reactions 1 to 4 are given in Figure 1. As it can be appreciated in Figure 1a, the dominant reaction is that giving $[HBr{-}Na]^+$ (reaction 2), its excitation function displaying a maximum at ∼3.0 eV and showing a relatively well-defined energy threshold at ∼0.30 eV. The excitation function for the formation of the $[C_3H_6{-}Na]^+$ by reaction 1 shows a much lower reactivity than that for reaction 2 with an experimental threshold energy of ∼0.1 eV. The shape of both excitation functions is the expected one for reactions with an energy threshold requirement. The same figure shows also the excitation function associated with the formation of the ion−molecule adduct, which decreases when the collision energy increases, as expected in a barrierless ion−molecule reaction. Figure 1b shows the excitation function for the decomposition reaction 3, whose energy threshold and maximum are at ∼0.90 and 3.50 eV, respectively. In the same figure, cross-section values for the $C_3H_7^+$ decomposition as a function of the collision energy according to reaction 4 are also shown, appearing at ∼4.00 eV. In comparing these results it follows that the highest cross section in collisions between $Na^+$ and $i\text{-}C_3H_7Br$ corresponds to the decomposition reaction in the energy range considered.

**2.3. Experimental Reactive Excitation Function in $Na^+ + i\text{-}C_3H_7OH$ Collisions.** As for the previous system, a mass scan in the same mass/charge unit range at different collision energies was done for the $Na^+ + i\text{-}C_3H_7OH$ system. Signals of varying intensity were observed at 83, 65, 41, 43, and 27 mass/charge ratio which, taking into account the chemical nature of the reactive system, can be associated with the ion−molecule reactants adduct $[Na{-}i\text{-}C_3H_7OH]^+$, products reaction channels


DOI: 10.1021/acs.jpca.5b11869
J. Phys. Chem. A XXXX, XXX, XXX−XXX

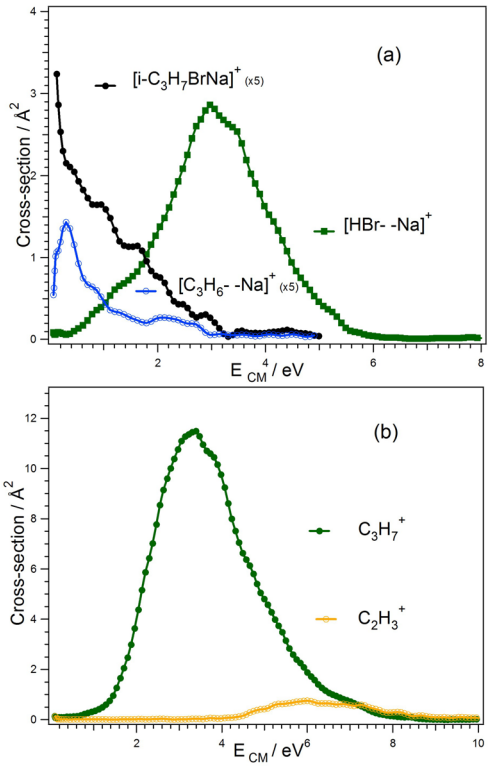


**Figure 1.** Reaction cross-section as a function of the CM collision energy for the formation of (a) the $[Na{-}i\text{-}C_3H_7Br]^+$ adduct and the $[HBr{-}Na]^+$ and $[C_3H_6{-}Na]^+$ reaction products and (b) the decomposition products $C_3H_7^+$ and $C_2H_3^+$ in the $Na^+$ + $i\text{-}C_3H_7Br$ collision system. Cross sections for $[Na{-}i\text{-}C_3H_7Br]^+$ and $[C_3H_6{-}Na]^+$ are multiplied by five (×5) as shown in the figure.

adducts $[C_3H_6{-}Na]^+$ and $[H_2O{-}Na]^+$, reactions 1 and 2, respectively, as well as the ions $C_3H_7^+$ (43 *m*/*z* units) resulting from the decomposition reaction 3 and $C_2H_3^+$(27 *m*/*z* units) from reaction 4. It is worth noting that, although the $[C_3H_6{-}Na]^+$ reaction product was detected, its associated measured intensity in the range of energies of the experiment was extremely weak so that the large uncertainties in the signal-to-noise ratio precluded measuring the cross-section energy dependence for reaction 1.

The CM excitation functions for reactions 1 to 4 are shown in Figure 2. In Figure 2a the cross-section energy dependence for the $[Na{-}i\text{-}C_3H_7OH]^+$ adduct formation at the lowest energy range is shown. Its global shape is the expected one for the barrierless formation of an ion−molecule adduct. In Figure 2b the excitation function for the $[H_2O{-}Na]^+$ formation by collision-induced alcohol dehydration (2) is given. In this case an energy threshold appears at ∼1.20 eV, cross-section values then increasing monotonously until a maximum at ∼4.50 eV. After this maximum, cross sections decrease uniformly, tending to disappear at collision energies high enough. In Figure 2c the measured cross-section values for reaction 3 are plotted as a function of the CM collision energy. The shape of this curve is also in agreement with that expected for a decomposition reaction, but the large experimental uncertainties at the lowest energies precluded measuring precisely its threshold energy, the nearest estimation made by extrapolating experimental data being ∼1 eV. In Figure 2c the energy dependence for reaction 4 is also given, showing clearly an experimental energy threshold of ∼2.50 eV and a maximum at ∼5.50 eV. From data shown in

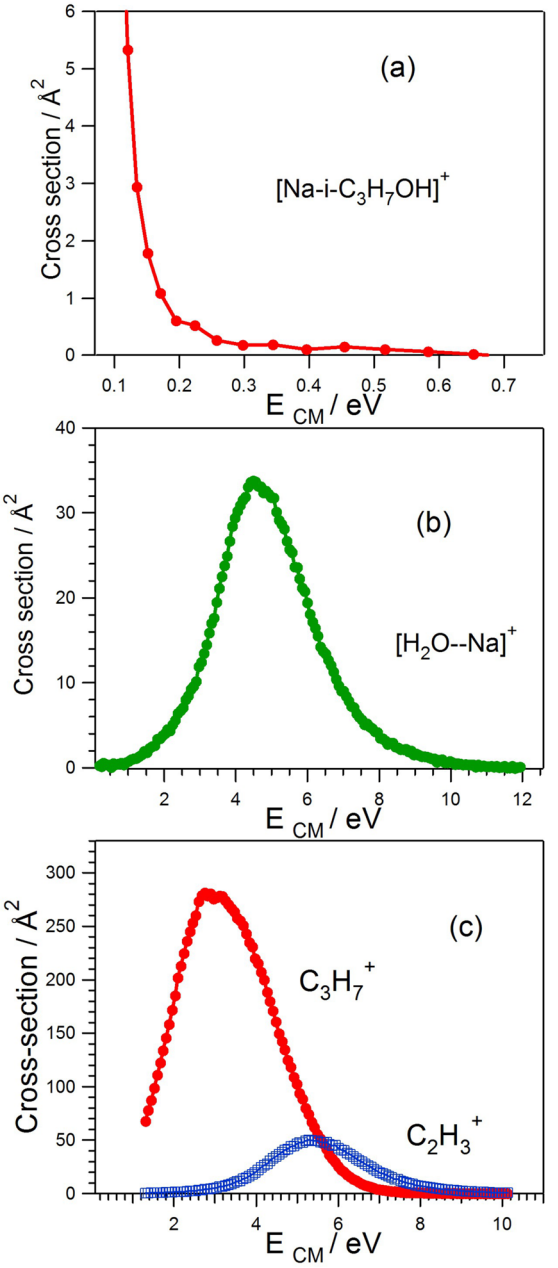


**Figure 2.** Reaction cross-section as a function of the CM collision energy for the formation of (a) $[Na{-}i\text{-}C_3H_7OH]^+$ adduct, (b) $[H_2O{-}Na]^+$ reaction product, and (c) $C_3H_7^+$ and $C_2H_3^+$ decomposition products in the $Na^+$ + $i\text{-}C_3H_7OH$ collision system.

Figure 2 and considering the range of energies studied, it can be seen that the decomposition reaction 3 has again the highest cross-section values at CM energies larger than 1.00 eV, while adduct formation is significantly measured only at energies below 0.50 eV.

## 3. QUANTUM CHEMISTRY CALCULATIONS

The experimental behavior of elementary chemical reactions is essentially controlled by the intermolecular forces established between the reacting partners along the reactive process. Moreover, the system's total energy content plays a decisive role on which products can be formed and on the possibility of their being detected experimentally. In the case of gas-phase reactions such as those that are the subject of the present work,


DOI: 10.1021/acs.jpca.5b11869
J. Phys. Chem. A XXXX, XXX, XXX−XXX

Table 1. MP2 Calculated Energies[a] ($\Delta E$), Zero-Point Energies[a] ($\Delta$ZPE), and Standard Reaction Enthalpies[a] ($\Delta_r H_0$), Referred to the Corresponding Reactants Values for the Different Minima (M), Transition States (TS), and Reactions 1, 2, and 3 Located on the Reactive Potential Energy Surface of the $(NaC_3H_7Br)^+$ System (see Figure 3)

| | M1 | TS1 | M2 | TS2 | M3 | (1) | (2) | (3) |
|---|---|---|---|---|---|---|---|---|
| $\Delta E$ | −1.072 | 0.317 | 0.072 | 0.157 | −0.202 | 0.474 | 0.567 | 1.752 |
| $\Delta$ZPE | 0.011 | −0.151 | −0.181 | −0.194 | −0.190 | −0.221 | −0.217 | −0.153 |
| $\Delta H_0$ | −1.061 | 0.166 | −0.109 | −0.037 | −0.392 | 0.253 | 0.350 | 1.599 |

[a]All values are given in electronvolts.

Table 2. MP2 Calculated Energies[a] ($\Delta E$), Zero-Point Energies[a] ($\Delta$ZPE), and Standard Reaction Enthalpies[a] ($\Delta_r H_0$), Referred to the Corresponding Reactants Values for the Different Minima (M), Transition States (TS), and Reactions 1, 2, and 3 Located on the Reactive Potential Energy Surface of the $(NaC_3H_7OH)^+$ System (see Figure 4)

| | M1 | TS1 | M2 | TS2 | M3 | (1) | (2) | (3) |
|---|---|---|---|---|---|---|---|---|
| $\Delta E$ | −1.415 | 1.323 | −0.755 | −0.722 | −1.048 | 0.147 | −0.347 | 3.659 |
| ZPE | 0.031 | −0.187 | −0.095 | −0.107 | −0.117 | −0.184 | −0.144 | −0.258 |
| $\Delta H_0$ | −1.384 | 1135 | −0.851 | −0.830 | −1.164 | −0.037 | −0.491 | 3.400 |

[a]All values are given in electronvolts.

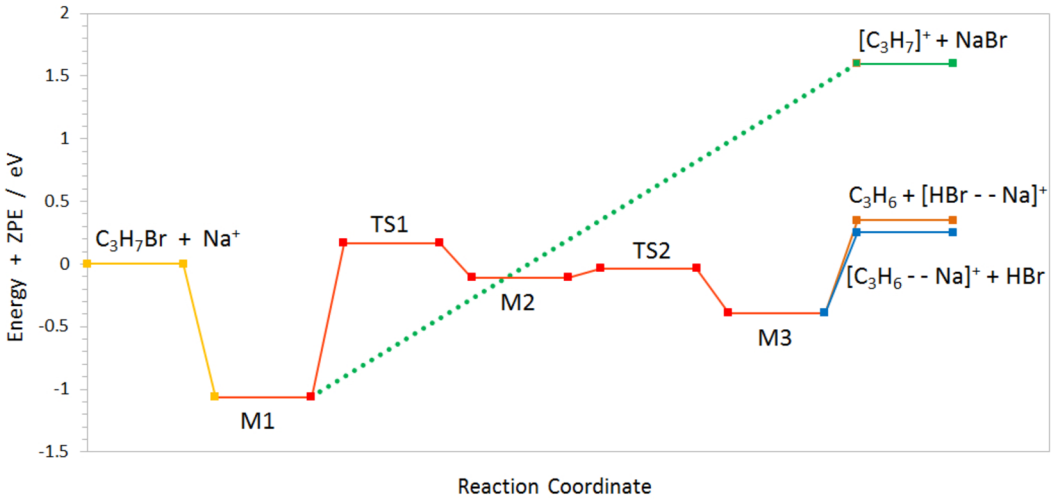


**Figure 3.** Schematic ZPE profile along the reaction path characterized at the quantum chemistry MP2 level on the singlet ground state of the $Na^+$ + $i$-$C_3H_7Br$ collision system (taking the reactants' ZPE as origin). The different minima (M) and transition states (TS1) located on the PES and their IRC connectivity are shown: Continuous (yellow) describes the reaction path from asymptotic reactants to the adduct M1; continuous (red) line describes the reaction path in the intermediate interaction region from M2 to M3; continuous (blue) and (orange) lines show the connectivity of M3 to the asymptotic reaction products (1) and (2). Dotted (green) line shows the reaction path for the decomposition reaction 3 from M1 to the asymptotic product region on the PES.

quantum chemistry methods[23] have proved to be an important tool for describing and understanding interactions between reactants, and they give detailed information on the PES where elementary processes take place. For the systems considered here, since the electronic structures of all reactants and products show a closed-shell configuration, it can be assumed that the reactive collisions described by reactions 1 to 4 evolve adiabatically, correlating asymptotically reactants and products and, consequently, that all reactions proceed on the ground singlet PES of the supermolecule system $(Na{-}i\text{-}C_3H_7R)^+$ (R = Br, OH). With the goal of fully characterizing the PES for both reactive molecules, their main topology features were obtained by performing ab initio calculations at the second order Möller-Plesset (MP2)[24] level of theory using the electronic structure Gaussian program package[25] and the Pople's 6-31G basis set including $p$ polarization functions for each hydrogen atom and $p$ polarization functions on each heavy atom as implemented in the computer code. The relevant stationary points on the ground singlet PESs of both reactive systems were localized using the reaction coordinate method[26] and the reaction path (RP),[27] exploring PESs along the reaction pathway. Moreover, the connectivity of the different stationary points along the RP was confirmed by applying the intrinsic reaction coordinate method (IRC)[28] to both potential energy hypersurfaces.

**3.1. Quantum Chemistry Results of the $(Na{-}i\text{-}C_3H_7R)^+$ with R = Br, OH Supermolecule Reactive System Potential Energy Surfaces.** Before proceeding to perform the above-mentioned PESs ab initio calculations, the geometry structures of the reactants and product for reactions 1 to 3 were determined as well as their corresponding electronic energies and zero-point energies (ZPE), so that reaction energies and standard reaction enthalpies at 0 K can be calculated. After characterizing reactants and products for both $(Na{-}i\text{-}C_3H_7R)^+$ systems, we proceeded to localize the stationary points on the respective PES asymptotically correlating reactants and products. Full characterization of these points was done by a detailed Hessian matrix analysis allowing their classification either as minima (M) or as transition states (TS) on the


DOI: 10.1021/acs.jpca.5b11869
J. Phys. Chem. A XXXX, XXX, XXX−XXX

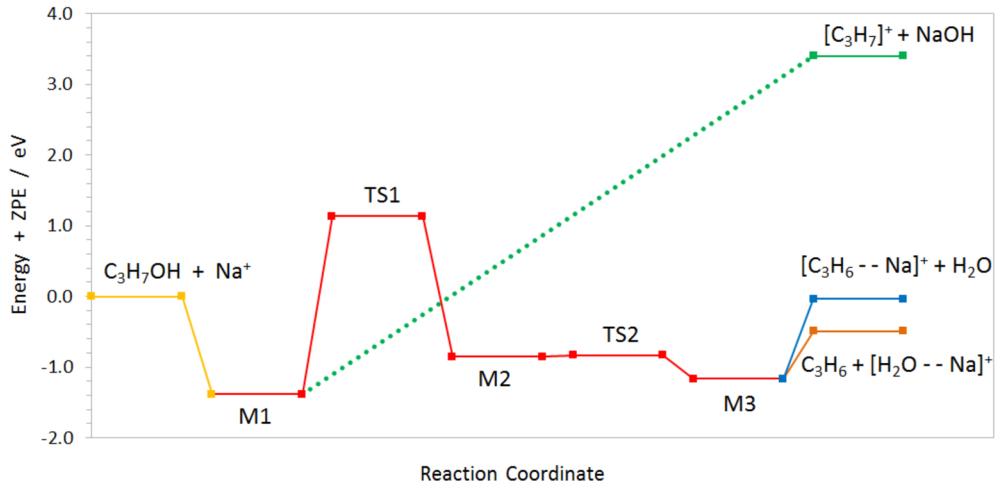


**Figure 4.** Schematic ZPE profile along the reaction path characterized at the quantum chemistry MP2 level on the singlet ground state of the $Na^+$ + *i*-$C_3H_7OH$ collision system (taking the reactants' ZPE as origin). The different minima (M) and transition states (TS1) located on the PES and their IRC connectivity are shown: Continuous (yellow) describes the reaction path from asymptotic reactants to the adduct M1; continuous (red) line describes the reaction path in the intermediate interaction region from M2 to M3; continuous (blue) and (orange) lines show the connectivity of M3 to the asymptotic reaction products (1) and (2). Dotted (green) line shows the reaction path for the decomposition reaction 3 from M1 to the asymptotic product region on the PES.

calculated PESs, and the connectivity between them was proved by means of the IRC procedure.

Taking as a reference the calculated energies and ZPEs for separate reactants, energies ($\Delta E$) and standard enthalpies ($\Delta H$) were calculated for each stationary point (M or first-order TS) located on the PESs, as well as the standard reaction enthalpies ($\Delta_r H_0$) for reactions 1 to 3 for both collision systems. Tables 1 and 2 give the $\Delta E$, $\Delta H$, and $\Delta_r H_0$ values at the MP2 level of theory for reactive systems $(Na{-}i\text{-}C_3H_7Br)^+$ and $(Na{-}i\text{-}C_3H_7OH)^+$, respectively. Figure 3 shows a schematic representation of the stationary points localized on the PES for the $(Na{-}i\text{-}C_3H_7Br)^+$ system along the RP. This gives detailed information on the PES most relevant topology effects. The data given in Table 1 demonstrate that channels (1), (2), and (3) in $Na^+$+ *i*-$C_3H_7Br$ collisions are both endoergic and endothermic, $\Delta_r H_0$ values for reactions 1 and 2 being ~0.22 eV lower than their respective $\Delta_r E$ values, while for reaction 3 this difference is only ~0.15 eV. This endoergic (and endothermic) character can also be observed in the reaction energy profile shown in Figure 3, which also evidence the presence of three minima M1, M2, and M3 associated with potential energy wells on the PES. From this figure and Table 1 data, it can be seen that a potential energy barrier corresponding to a first-order transition state (TS1, with a 370.64*i* $cm^{-1}$ imaginary frequency) is located on the PES separating M1 and M2 minima. Similarly, a transition state barrier (TS2, with 203.66*i* $cm^{-1}$ imaginary frequency) separates potential energy wells M2 and M3. As clearly evidenced by Figure 3, in both the PES' reactants and products zones and before reaching the respective asymptotic channels, potential energy well M1 can be assigned to an adduct produced by the association of the sodium ion with the neutral 2-bromopropane molecule, while M3 could be related with product adducts and linked to the interaction between neutral and ionic reaction products. In both Table 1 data and Figure 3 it can be seen that ZPEs for reaction products (1) and (2) are higher than the ZPE of the higher energy transition state TS1 and that M2 is the shallowest of the three potential energy wells localized on the PES along the reaction evolution from reactants to products. Also, in the same figure and table it can be seen that the decomposition reaction 3 is the most endoergic (and endothermic) one, products being formed through an adiabatic evolution of the $(Na{-}i\text{-}C_3H_7Br)^+$ supermolecule from M1 to the asymptotic region of the PES describing this reaction channel.

For the $(Na{-}i\text{-}C_3H_7OH)^+$ reactive system a schematic representation of the stationary points located on the adiabatic PES of the $Na^+$ + *i*-$C_3H_7OH$ reactive collisions along the reaction evolution is given in Figure 4 showing its main topology characteristics. From this and from data given in Table 2 it can be seen that reactions 1 and 3 are endoergic, while (2) is exoergic. When the respective ZPEs are included, reaction 1 becomes slightly exothermic, while reactions 2 and 3 maintain their relative characters, (2) being exo- and (3) endothermic at 0 K. In this system, reaction 3 shows a higher endothermicity than the equivalent one in $Na^+$ + *i*-$C_3H_7Br$ collisions. For $Na^+$ + *i*-$C_3H_7OH$, Figure 4 shows also the presence of three potential energy wells (M1, M2, and M3) and two potential energy barriers associated with first-order transition states, TS1 and TS2, with imaginary frequencies 1322.18*i* $cm^{-1}$ and 62.19*i* $cm^{-1}$, respectively. TS1 is located between M1 and M2, all of them being connected by the corresponding IRC path, and TS2 separates M2 from M3 also connected along its own IRC path. As can be appreciated from both Figure 4 and Table 2 data, TS2 barrier height is only 0.021 eV referred to the M2 minimum, practically 3.5 times lower that the equivalent TS2 barrier in the $(Na{-}i\text{-}C_3H_7Br)^+$ system. Probably the most striking feature in Figure 4 is the high potential energy of TS1, ~1.0 eV higher than its homologue in the $(Na{-}i\text{-}C_3H_7Br)^+$ PES, this energy barrier being significantly above the asymptotic energies of reactions 1 and 2. Potential energy minima M1 and M3 in the same figure, as in the case of the bromide-ion collisions, can be associated with ion–molecule adducts, M1 standing for the reactants adduct $[Na{-}i\text{-}C_3H_7OH]^+$ and M3 for the product ones, $[C_3H_6{-}Na]^+$ and $[H_2O{-}Na]^+$ in 1 and 2, respectively. Moreover, potential energy wells M1, M2, and M3 on the ion-alcohol PES are noticeably deeper than their homologues in the ion-bromide as


DOI: 10.1021/acs.jpca.5b11869
J. Phys. Chem. A XXXX, XXX, XXX–XXX

can be seen from data in Tables 1 and 2. As is also the case for the ion-bromide system, the calculated endothermicity for (3) is relatively high, higher in fact by ∼1.80 eV than that for reaction 3 in the $(Na-i\text{-}C_3H_7Br)^+$ PES. While the $\Delta_rH_0$ value calculated for 3 (see Table 1) in ion-bromide collisions agrees well with that estimated from formation enthalpies[29−31] (1.51 eV), for ion-alcohol the calculated $\Delta_rH_0$ value for 3 (Table 2) is 0.61 eV larger that the estimated one (2.79 eV).

**3.2. Quantum Chemistry Structures of the Relevant Stationary Points on the Reactive Potential Energy Surface of the $(Na-i\text{-}C_3H_7Br)^+$ System.** The geometry structures associated with the different stationary points on the PES and those for reactants and reaction products relevant to reactions 1 to 3 in the $Na^+ + i\text{-}C_3H_7Br$ colliding system, are shown in Figure 5 where, to simplify, only the most significant interatomic distances are given. From Figure 1a and for reaction 1, the $[C_3H_6-Na]^+$ structure can be seen where the sodium ion interacts with the propene C=C bond. $Na^+$ and the double bond carbons lie in a plane practically orthogonal to that defined by the propene three carbon atoms, its distance to the central one being 0.182 Å shorter than that between sodium and terminal carbon. The longer $Na^+$−central carbon distance can be explained in terms of Coulomb interactions, considering that in this adduct sodium supports a charge of +0.889 units (calculated as the atomic polar tensor (APT) charges[32]); the central carbon charge is +0.037 units, while the terminal one is −0.189 units. This negative charge promotes the sodium−terminal carbon atom attraction against the sodium−central carbon repulsion. For the $[C_3H_6-Na]^+$ adduct the calculated C=C bond length is 0.013 Å larger that the corresponding one in isolated $C_3H_6$; this increase can be interpreted in terms of the globally larger repulsive Coulomb interaction between the three charged atoms (Na−C=C) in comparison with the double bond in isolated propene, whose calculated equilibrium distances (see Figure 1a) agree very well with the available data.[31] C−H distances in the $[C_3H_6-Na]^+$ adduct do not change significantly with respect to those in propene. A detailed analysis of the calculated ab initio molecular orbitals (m.o.) shows that the atomic orbitals of the sodium atom do not contribute significantly to the valence shell m.o. in the $[C_3H_6-Na]^+$ adduct, the $Na^+-C_3H_6$ interaction thus being essentially noncovalent, as is also the case for other alkali ion-neutral molecules.[33] For reaction 2 quantum chemistry calculations give a practically right-angle configuration for the $[HBr-Na]^+$, where bromine has a −0.135 unit charge and is coordinated to the sodium ion with a +0.943 unit net charge. In this adduct the presence of the coordinated sodium ion leaves the Br−H bond distance practically undistorted respect to the equilibrium gas-phase distance (1.414 Å).[29] The analysis of the m.o. of the triatomic adduct shows essentially no contribution of the sodium orbitals in the valence-occupied m.o. The interaction is established mainly between a nonbonding *p* orbital of the bromine atom and the closed-shell sodium ion, thus justifying the practically right-angle bond of the three-center molecule. In Figure 5a the calculated geometrical structures for the $C_3H_7^+$ and NaBr reaction products (3) are given. Results for the former molecule are in agreement with a study on $C_3H_7^+$ decomposition previously done by some of the authors.[34] This molecular ion shows the so-called classical structure, with a central carbon partial charge of +0.735 units and −0.334 units for both adjacent carbons, while those for hydrogens range between +0.106 and +0.165 units except that for the central one, which is slightly lower at +0.089 units. For the NaBr neutral product the calculated internuclear distance agrees quite well with reported data (2.502 Å),[29] while calculated APT partial charges are symmetrically distributed on the Na (+0.767 units) and Br (−0.767 units) atoms with an associated dipole moment for the NaBr molecule of 9.289 D in agreement with reported data (9.092 D).

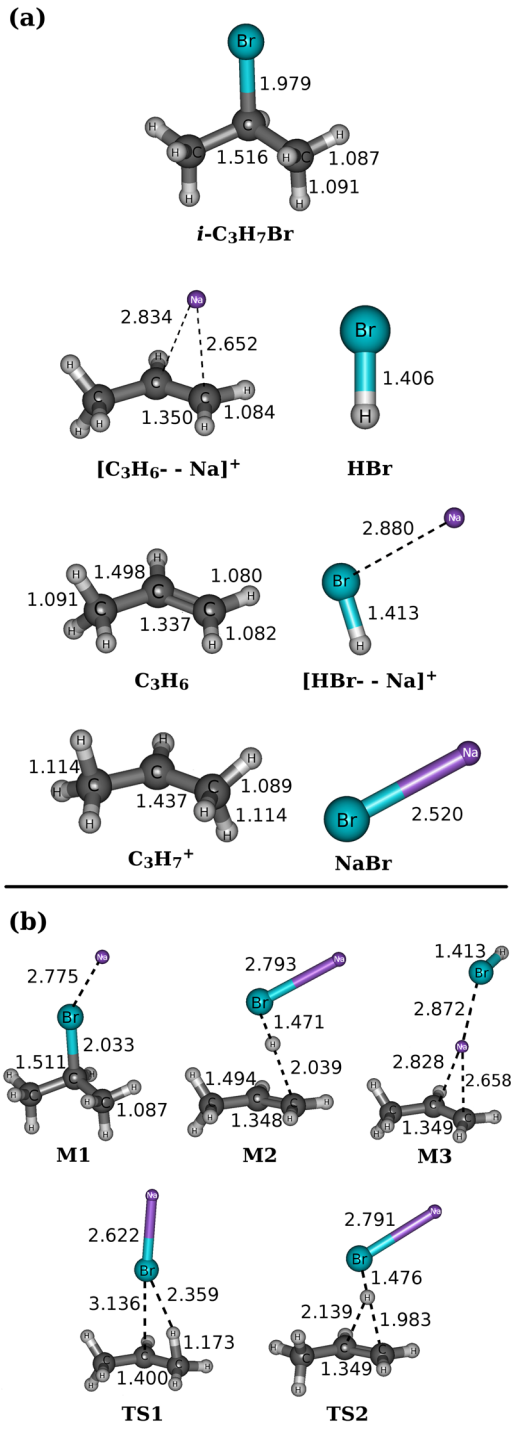


**Figure 5.** Optimized geometry structure at the quantum chemistry MP2 level of the different molecular structures involved in $Na^+ + i\text{-}C_3H_7Br$ collision system: (a) Structures for the reactant molecule and the different reaction products; (b) Structures associated with the different stationary points localized on the PES, minima (M) and transition states (TS).


DOI: 10.1021/acs.jpca.5b11869
J. Phys. Chem. A XXXX, XXX, XXX−XXX

In addition to the products' geometric structures, those associated with the stationary points localized on the PES of the $(Na-i\text{-}C_3H_7Br)^+$ system are also given in Figure 5b. The optimized equilibrium structure in M1 shows that the $Na^+-i\text{-}C_3H_7Br$ adduct has the sodium ion coordinated to the bromine atom at 2.775 Å, while central carbon−bromide and carbon−carbon distances are only slightly increased (0.054 Å) and decreased (0.005 Å), respectively, in comparison with the same in isolated $i\text{-}C_3H_7Br$. The ion molecule interaction is also noncovalent, as corroborated by the analysis of the adduct valence m.o. and of the charge distribution, which show no significant contribution from the sodium orbitals. The interaction is created between the bare sodium ion and the nonbonding orbitals of the bromine atom, whose partial charges are +0.923 and −0.454 units, respectively, and which reflects a small decrease (~0.077 units) of the $Na^+$ initial charge. The $Na^+$ approach to the neutral molecule to form the M1 structure modifies its charge distribution, increasing the central carbon charge fraction from +0.396 to +0.565 units and the bromine negative one from −0.310 to −0.435 units. Such charge redistribution between ion and molecule without forming covalent interactions indicates that the forces controlling the reactants' interaction are essentially noncovalent and mainly electrostatic in character. Following the reaction pathway from M1 to TS1, it can be seen that the Na ion coordinated to the Br atom plays a role in weakening the bond between the bromine and the central carbons, the methyl group rotating around the C−C bond, enhancing the interaction between bromine and the approaching active hydrogen, also weakening the initial C−H bond that lengthens to 0.086 Å, and finally reaching the structure shown in TS1. In this transition state, charges on central carbon, Br and Na are +0.643, −0.895, and +0.891 units, respectively, the central carbon increasing its positive charge, bromine also increasing its negative one and sodium decreasing its positive charge compared to those for M1. From TS1, the system evolves to the M2 structure, where (see Figure 5b) the active hydrogen has increased its C−H distance in 0.952 Å, being practically nonbonded to the terminal carbon atom, while its distance to the bromine is very close to the calculated HBr equilibrium one (1.406 Å, see Figure 5a). Moreover, the M2 structure shows that the central-terminal carbon double bond has already formed and that its bond distance is only slightly distorted (0.011 Å) with respect to its equilibrium value in the $C_3H_6$ molecule. In M2 structure associated with the carbon skeleton the charge fraction on the central carbon is +0.012, and −0.235 on the terminal one; for the HBrNa subsystem, charge fractions for H, Br, and Na are +0.565, −0.482, and +0.825, respectively. From the shallow minimum M2 the reacting supermolecule evolves to the TS2 configuration where the triatomic subsystem HBrNa reorients itself with respect to M2, while the charge distribution remains essentially unaltered with respect to the M2 one. Surmounting the potential energy barrier associated with TS2 the system evolves into the M3 structure that, as can be appreciate in Figure 5b, can be associated with the formation of an adduct where the sodium ion is simultaneously coordinated to the propene's C=C bond by one side and to the HBr bromine by the other. In this structure, charges on the central and terminal carbons are +0.063 and −0.186, respectively. Charges on sodium, bromine, and hydrogen atoms in the triatomic subsystem NaBrH are +0.837, −0.135, and +0.188, respectively. In view of the relatively large size of the $C_3H_6$ and HBr fragments as well as of their small net charge (+0.109 and +0.054, respectively), M3 space distribution can be interpreted as if both fragments were trying to minimize their mutual repulsive interactions. As can be appreciated in Figure 5b the $Na^+$ distances to both $C_3H_6$ and HBr fragments in M3 are relatively large, so it can be expected that interactions between the ion and each fragment are mainly noncovalent, as was confirmed from the analysis of the adduct m.o., without any important overlapping between the different fragments.

### 3.3. Quantum Chemistry Structures of the Relevant Stationary Points on the Reactive Potential Energy Surface of the $(Na-i\text{-}C_3H_7OH)^+$ System.

In Figure 6 the geometrical structure of the different stationary points located along the reaction path from reactants to products on the PES reaction profile for the $(Na-i\text{-}C_3H_7OH)^+$ system is given together with those of reactants and products, while common reaction products described in the isopropyl bromide reaction were omitted. Comparing the geometry of the 2-hydroxypropane (Figure 6a) with the equivalent bromine derivative it can be seen that C−C and C−H bond distances are quite similar in both reactants, but the central carbon−oxygen distance is much

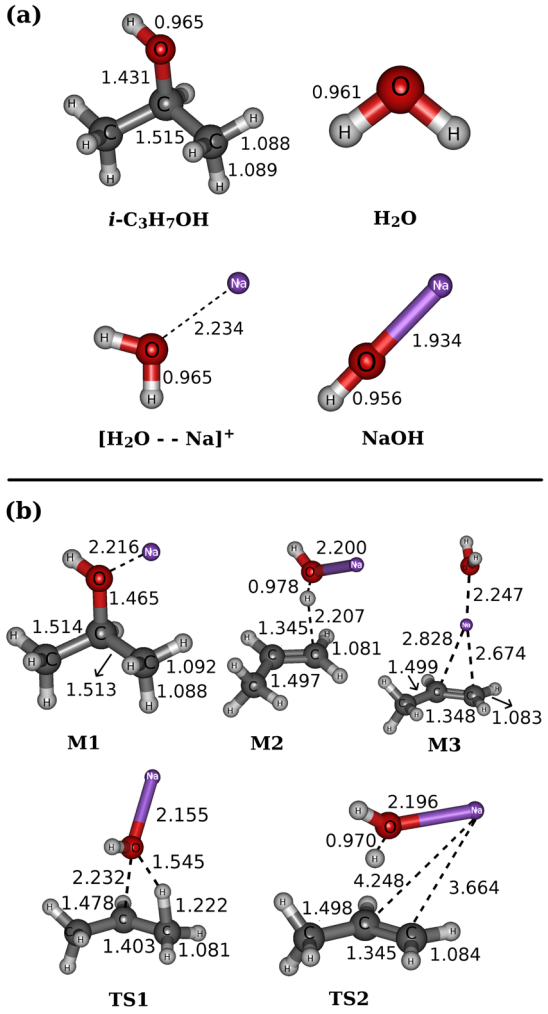


**Figure 6.** Optimized geometry structure at the quantum chemistry MP2 level of the different molecular structures involved in $Na^+ + i\text{-}C_3H_7OH$ collision system. (a) Structures for the reactant molecule and for the different reaction products. (b) Structures associated with the different stationary points localized on the PES, minima (M), and transition states (TS).


DOI: 10.1021/acs.jpca.5b11869
J. Phys. Chem. A XXXX, XXX, XXX−XXX

shorter than the corresponding one in the bromine compound. Calculated ATP charges on central carbon (+0.538) and oxygen atoms (−0.609) are larger than those on central carbon and bromine in isopropyl bromide (+0.396 and −0.309, respectively). The same figure shows also the structure of the planar $[H_2O–Na]^+$ adduct. Its H−O distance (0.965 Å) and H−O−H angle (104.8°) being both very close to those of the free water molecule (0.961 Å and 103.8°, respectively), and the bond distances for the linear NaOH (product in reaction 3) are in good agreement with available data basis.[35] In the $[H_2O–Na]^+$ adduct the +0.961 sodium charge causes some increase in the charges on the oxygen (−0.655) and hydrogen (+0.345) atoms with respect to those in the water molecule (−0.521 and +0.260, respectively), while charge distribution for the linear NaOH was found to be +0.732 for Na, −0.883 for O, and +0.151 for H.

The geometric structure of the $[Na–i\text{-}C_3H_7OH]^+$ adduct is given In Figure 6b. We can see that the sodium is attached to the oxygen atom at a relatively large distance, while the H, O, central C, terminal C, and Na atoms are practically coplanar. In this M1 adduct, C−C and C−H bond lengths have practically the same values as in the isopropyl alcohol, while the C−O distance is slightly increased (0.034 Å) due to its interaction with the sodium ion. The ion−molecule interaction leads to sodium having a +0.933 charge in M1 that induces a slight variation from the distribution in the original O−H, the oxygen charge changing from −0.609 in the alcohol to −0.736 in the adduct, and that on hydrogen from +0.239 to +0.293, while the remaining charges remain practically unchanged. As in the case of the M1 adduct considered in the former reaction, the m.o. analysis indicates that noncovalent interactions play a major role in the formation of the ion−molecule adduct. From the M1 potential energy well the supermolecule evolves toward products, reaching a true saddle point on the PES (TS1 in Figure 6b) with a relatively high ZPE potential energy barrier as can be appreciated from Figure 4. It can be seen there that the central C−OH bond distance has increased notably (0.80 Å) with Na clearly interacting with the OH group via the oxygen and announcing the formation of NaOH with a distorted angular geometry (Na−O−H angle ≈ 111.3°; see Figure 6b). At the same time the oxygen atom approaches the active H atom of a methyl group, with the central carbon, the methyl C, the active H, and the oxygen being all located on the same plane, practically perpendicular to the H−O−Na plane. The increase of the central C−O distance modifies notably the charge on both atoms, that on the central carbon increasing to +0.793 and that on the oxygen to −1.050, in agreement with the more electronegative character of the oxygen atom in the C−OH bond, both charge increments almost compensating. The charge fraction on the hydrogen atom of the O−H group decreases from +0.293 to +0.188, the Na charge fraction in TS1 (+0.907) is close to that displayed in the M1 structure, while other atoms also show small (in general below 0.1 units) changes in their charge distribution in this transition state structure. From TS1 the supermolecule structure evolves to that corresponding to potential energy well M2, whose geometry structure is shown in Figure 6b. It can be seen that a C═C double bond is practically formed with a bond length differing only 0.008 Å with respect to the same bond for the calculated $C_3H_6$ molecule (see Figure 5a), and the distance of the active hydrogen to the original terminal carbon atom (2.207 Å) is practically 1 Å greater than in the TS1 structure. In the M2 structure the plane of the HOHNa fragment also contains one of the C−H bonds in the terminal unsaturated C atom. Moreover, this plane is practically perpendicular to that defined by propene's three carbon atoms. The more pronounced charge fraction changes in M2 with respect to the TS1 structure are: sodium increases its charge to +0.947, the central carbon decreases theirs to +0.038, and oxygen also decreases to −0.763. Such a charge distribution points out that, while the supermolecule conserves its positive global charge, the M2 structure can be seen as resulting from the interaction between the near-formed, practically uncharged $C_3H_6$ subsystem (with a very small +0.05 global charge fraction) and the positively charged $NaOH_2^+$ subsystem (with a +0.95 charge). From the M2 structure the reactive supermolecule evolves to the final M3 minimum after surmounting the small ZPE potential energy barrier (0.012 eV) associated with TS2, whose geometry structure is also given in Figure 6b. As it is shown there, in TS2 structure the planar $NaOH_2$ system reorients itself relative to the $C_3H_6$ carbon skeleton, both planes being disposed practically at right angles and the charge fraction distribution being quite close to the TS2 one. The evolution from TS2 to M3 leads to a stabilization of the supermolecule that is only 0.220 eV less stable than the ion−molecule reactants adduct M1. From Figure 6b it can be seen that the structure evolution from TS2 to M3 involves a restructuration of the four-center subsystem such that the Na atom is resituated on top of the C═C double bond, and in turn the water molecule moves away from the propane subsystem redirecting the sodium−water plane that is virtually located perpendicularly to the plane of the propane skeleton. In the M3 structure the $Na^+$ appears as coordinated to the $C_3H_6$ molecule in a given direction and to the water molecule in the opposite one. As can be appreciated from the M3 structure in Figure 6b the sodium ion is located almost but not exactly symmetrical to the double bond carbons and closer to the terminal one, the corresponding distances being notably shorter than the equivalent ones in TS2, while Na−O distance increases slightly to 0.051 Å and the C−C and C−H ones do not change significantly. Charge distribution on carbon and hydrogen atoms remains practically unchanged, while charges for sodium and oxygen increase slightly (~0.1 or less) to +0.864 and to −0.640, respectively. As in the case of M1 and M2, interaction between the sodium atom and coordinated subsystems is essentially noncovalent in nature. The final reaction products (1) and (2) can be reached from M3 minimum as will be commented on in the next section.

## 4. DISCUSSION ON THE DEHYDROHALOGENATION AND DEHYDRATION REACTIONS

A deep, full understanding of elementary chemical reactions requires knowledge of the interaction forces among participants and the dynamics of the reactive processes. In the absence of dynamical simulations of the collision systems described here, quantum chemistry calculations such as those shown in the third section can give information helping to interpret, at least qualitatively, the experimental measurements described in Section 2. As is well-known, experimental measurements can be correlated with the most relevant topologic features of the PES where reactions, such as those in this article, are assumed to evolve adiabatically. For both systems studied here, the fact that reactants can reach M1 without overcoming any potential energy barrier leads to expect the formation of the respective ion−molecule adducts which were measured experimentally at 146 and 83 $m/z$ units for the bromide and the alcohol, respectively, their cross-section values not showing any energy


DOI: 10.1021/acs.jpca.5b11869
J. Phys. Chem. A XXXX, XXX, XXX−XXX

threshold. For both reactions and for collision energies below the TS2 energy height, the M1 adduct, produced with a relatively high vibrational energy content ($T \rightarrow V$), can either become quickly stabilized (usually in the picoseconds time scale[27]) by redistributing its energy among the different vibrational modes and emitting infrared photons (not measured in the present experimental setup) or alternatively can decompose, back-dissociating into reactants. Taking into account that these processes are very fast and that under experimental conditions the adducts formed in the reaction cell reach the detector in $\sim 1 \times 10^{-3}$ to $1 \times 10^{-4}$ s, a decreasing cross-section energy dependence can be expected for adducts formation as corresponds to a barrierless ion−molecule reaction, and also as shown in the excitation functions plotted in Figures 1a and 2a. These show that cross-section values for the $[Na{-}i\text{-}C_3H_7OH]^+$ adduct are larger than those for the $[Na{-}i\text{-}C_3H_7Br]^+$ one but for the former its value rapidly decreases with energy while the latter's show a slower decrease. A possible explanation of this fact could be found in the lower potential energy barrier of TS2 in the bromide's case which allows M2 and M3 to be easily populated by species that, being different from M1, have the same $m/z$ value, so that measured cross sections gather the contribution of all of them.

The stronger ion−molecule interaction in the $[Na{-}i\text{-}C_3H_7OH]^+$ adduct could qualitatively explain its cross-section values being larger than the $[Na{-}i\text{-}C_3H_7Br]^+$ones, while the more complex M1 structure of the former adduct could facilitate its back-decomposition even at relatively low energy collisions leading to a faster decrease of the $[Na{-}i\text{-}C_3H_7OH]^+$ adduct excitation function.

As can be seen in Figure 3 and Table 1 the endothermicity of reactions 1 and 2 in $Na^+ + i\text{-}C_3H_7Br$ collisions is higher than the $\Delta H_0$ of TS1, so it can be expected that excitation functions for both reactions will show an energy requirement in agreement with the experimental energy dependences as plotted in Figure 1a. Although the small reactivities and the experimental uncertainties do not allow obtaining reliable energy thresholds, these can be roughly estimated to be ∼0.1 and 0.4 eV for reactions 1 and 2, respectively, agreeing well enough with calculated reaction endothermicity. As can be seen from Figure 1a, cross-section values for reaction 2 are of the order of few square angstroms, while those for reaction 1 are ∼1 order of magnitude lower in the range of collision energies studied. However, from a statistical interpretation of both reactions' reactivity and from their endothermicity, the more exothermic reaction 1 ought to be favored instead of (2). A plausible interpretation of this effect can be made by considering the geometry structure of the M2 collision complex (see Figure 5b) where reaction 2 products are actually formed simply by increasing the distance between the hydrogen of the HBrNa to the terminal double bonded carbon, so that the asymptotic $C_3H_6 + [HBr{-}Na]^+$ products are obtained. This reaction pathway[16] avoids the TS2 bottleneck associated with the M2 geometric rearrangement into the M3 one, which is required for the formation of reaction 1 products, at least in terms of an RP evolution. From M3 structure it can be seen that reaction 1 and 2 products can be obtained by lengthening the Na−BrH distance or the $Na{-}C_3H_6$ one, respectively, reaction 1 being thermodynamically favored.

For $Na^+ + i\text{-}C_3H_7OH$ both reactions 1 and 2 are exothermic, the energy requirement being in this case imposed by the notable height of the potential energy barrier associated with TS1. As stated in the Experimental Section it was not possible to measure with enough reliability the excitation function for the less exothermic reaction 1, while that for reaction 2 is given in Figure 2b, showing the profile expected for a reaction with an energy requirement. From an energy threshold that can roughly be estimated at ∼1 eV (in good agreement with calculated values) cross-section values increase with the collision energy, describe a maximum, and later decay until eventually disappearing at high energies. In the present case both the stronger exothermic character of reaction 2 compared to that of reaction 1 and the fact that the M2 internal rearrangement into M3, leading to reaction 2 products, can be avoided basically by the same considerations as in the dehydrohalogenation's case ($NaH_2O^+$ practically formed in M2 structure) can help to interpret the cross-section measures for $NaH_2O^+$ formation. All these considerations together with the $[C_3H_6{-}Na]^+$ dissociation energy, ∼0.02 eV lower than that for the $[H_2O{-}Na]^+$, could contribute to explain our inability to measure the corresponding excitation function.

For both systems, reaction 3 becomes possible at relatively high energies and, according with ab initio quantum chemistry calculations, proceed adiabatically on the ground singlet PES of the supermolecule system. According to these calculations reaction 3 can be seen as the heterolytic breakage of the covalent bond between the central carbon atom and the bromide (or hydroxyl) group induced by its interaction with the $Na^+$, both reactions being endothermic as shown in Figures 3 and 4. As can be seen in Table 1 the calculated $\Delta_r H_0$ value for reaction 3 in the $(Na{-}i\text{-}C_3H_7Br)^+$ system agrees well with that obtained (1.51 eV) from experimental data, while for $(Na{-}i\text{-}C_3H_7OH)^+$ the quantum chemistry value (see Table 2) is 0.61 eV higher than the experimental one (2.79 eV). However, results from calculations done under different approaches (basis sets with or without polarization functions, including or not core electron correlations) do not significantly differ from those given in Table 2, and for coherence all calculation results reported in Table 2 were obtained using the procedure outlined in Section 3. Considering the energy requirement for reaction 3 in both halide- and alcohol-derived molecules, measured excitation functions ought to have an energy threshold in agreement with experimental measurements as shown in Figures 1b and 2c. Taking into account the weak signals measured at threshold and near-threshold energies as well as the small signal-to-noise ratio in this energy range, by extrapolating experimental data we estimated threshold energies to values of ∼1.2 and 1.0 eV for $(Na{-}i\text{-}C_3H_7Br)^+$ and $(Na{-}i\text{-}C_3H_7OH)^+$, respectively, as shown in Figures 1b and 2c. The former value relatively agrees with ab initio predictions, but the latter is significantly (∼1.8 eV) lower than those calculated from the ab initio calculations and those estimated from experimental endothermicity.[35] This reduction of the experimental threshold energy values with respect to calculated ones could be justified considering that temperature in the reaction cell is ∼303 K. However, assuming an equilibrium statistical distribution of vibrational energy at working temperature, the vibrational energy excess over the respective ZPE (∼0.072 eV) does not help much in justifying the difference between reaction threshold energies, particularly in the case of the $(Na{-}i\text{-}C_3H_7OH)^+$ system.

As can be appreciated in Figures 1b and 2c after the energy threshold, excitation functions increase with energy, reaching a maximum at ∼4.40 eV for $(Na{-}i\text{-}C_3H_7Br)^+$ and 3.00 eV for $(Na{-}i\text{-}C_3H_7OH)^+$, later decreasing to nonsignificant values at ∼8.0 eV. In both cases and from a dynamics point of view,


DOI: 10.1021/acs.jpca.5b11869
J. Phys. Chem. A XXXX, XXX, XXX−XXX

reactions 3 are the dominant ones at relatively high collision energies according to their endothermic character, reactions 1 and 2 not significantly contributing to the global reactivity of both systems. The breakage of the C−R covalent bond requires not only a high-energy $(Na{-}i\text{-}C_3H_7R)^+$ collision complex but also an adequate energy distribution among the complex vibrational modes, so that the proper amount of energy can be channeled into the C−R bond. In the collision energy range where reaction 3 is dominant (roughly over 1 eV), the relatively low efficiency of reactions 1 and 2 results from the difficult redistribution of the supermolecule energy content among its internal vibrational degrees of freedom ($T \rightarrow V$), in particular, among those strongly related with its evolution along the reaction coordinate. Moreover, even if a reactive collision is evolving toward products in reactions 1 or 2, the high energy content of the supermolecule in the final stages of the collision process can lead to the alkali ion separating from the final reaction product to which it is coordinated ($C_3H_6$ and HBr for $i$-$C_3H_7Br$; $C_3H_6$ and $H_2O$ for $i$-$C_3H_7OH$). This effect leads to a loss of measured reactivity when the detected species are ions such as $[C_3H_6{-}Na]^+$, $[HBr{-}Na]^+$, and $[H_2O{-}Na]^+$. This effect was clearly evidenced and found in similar reactive systems previously studied in our research by running out direct quasiclassical trajectories.[36] Unfortunately, the high time consumption of these calculations does not allow us to run them for the systems described here. The decrease of the measured cross-section values after the maximum can also be interpreted, at least partially, in terms of the supermolecule losing its ability to efficiently couple vibrational modes and to channel energy into the C−R bond, likely as a consequence of the reduction of the coupling effect between vibration states at high energies.[37] Moreover, increasing the energy content of the supermolecule also increases the internal energies of the products, in particular, $C_3H_7^+$ that can then decompose in different ways.[38] As shown in Figure 1b and Figure 2c, at collision energies slightly higher than those for the excitation function maximum for the formation of $C_3H_7^+$, the production of a possible fragmentation product $C_2H_3^+$ is evidenced, the corresponding excitation functions showing the typical shape expected of chemical reactions with an energy requirement, in this case associated with the carbon−carbon bond breakage in $C_3H_7^+$ according with reaction 4, while other possible decomposition channels of excited $C_3H_7^+$ were not observed in the energy range studied. Cross-section values for reactions 4 are notably smaller than those for $C_3H_7^+$ formation, and their threshold energies, referred to those for formation of its parent ion, were estimated with a relatively large uncertainty from Figures 1b and 2c to be ∼2.8 eV for $(Na{-}i\text{-}C_3H_7Br)^+$ and 2.3 eV for $(Na{-}i\text{-}C_3H_7OH)^+$, these values being in agreement with previous quantum chemistry calculations[39] done by some of the authors.

Taking into account that in our experimental conditions the reactant gases inside the reaction cell are in thermal equilibrium at 303 K, an equilibrium distribution for their internal vibrational and rotational states can be assumed. Consequently, the measured cross-section at a fixed collision energy gives the contribution of all state-to-state cross sections added over all product states and statistically weighted over all reactant states at the experimental temperature. From experimental reactive excitation functions the corresponding thermal rate constants at a fixed temperature $k(T)$ can be calculated by properly averaging over a thermal collision energy distribution.[23] At 303 K the rate constants calculated for reactions 1 and 2 in the $Na^+ + i\text{-}C_3H_7Br$ reactive system were $5.1 \times 10^{-13}$ molecule$^{-1}$·cm$^3$·s$^{-1}$ and $2.6 \times 10^{-13}$ molecule$^{-1}$·cm$^3$·s$^{-1}$, respectively, and that for reaction 2 in the $Na^+ + i\text{-}C_3H_7OH$ collision system was $9.6 \times 10^{-9}$ molecule$^{-1}$·cm$^3$·s$^{-1}$. Neither one of these systems were explicitly considered by Allison and Ridge,[10] but calculated rate constants for reactions 1 and 2 in the case of the $i$-$C_3H_7Br$ are ∼2 orders of magnitude lower than the estimated upper limit on rate constants for systems they considered, while calculated rate constant for reaction 2 in the case of $i$-$C_3H_7OH$ is close enough to the order of magnitude they estimate for rate constants of the reactions discussed there.

Gas-phase dehydrohalogenation and dehydration of halogenated hydrocarbon derivatives and alcohols are an important subsection in the plethora of complex elimination reactions taking place when gases are heated at high temperatures, and they play an important role in complex chemical kinetics.[40] These decomposition reactions are commonly endothermic and in homogeneous conditions show relatively high activation energies in comparison to their endothermicity. For the $i$-$C_3H_7Br$ and $i$-$C_3H_7OH$ compounds considered here the corresponding elimination reaction enthalpies are 83.1 kJ mol$^{-1}$ (0.86 eV) and 50.8 kJ mol$^{-1}$ (0.53 eV), respectively, while their respective activation energies are 199.6 kJ mol$^{-1}$ (2.07 eV)[41] and 280.7 kJ mol$^{-1}$ (2.91 eV).[42] Gas-phase elimination reactions are unimolecular processes in which the energy requirement for overcoming the corresponding potential energy barrier is usually fulfilled by thermal collisions leading, in the present case, to the formation of $C_3H_6$ and either HBr or $H_2O$ products. Dehydrohalogenation and dehydration reactions reported in the present work are typical bimolecular collisions in which the alkali ion induces the elimination of HBr or $H_2O$ from $i$-$C_3H_7Br$ and $i$-$C_3H_7OH$, respectively, and the reaction energy requirement is furnished by the collision process transferring translational energy to the internal vibrational modes of the neutral target molecule ($T \rightarrow V$) along the evolution of the collision complex on the reaction PES to products. The essentially noncovalent interaction of the sodium ion with neutral molecules is strong enough to notably perturb the PES on which gas-phase molecules experience unimolecular elimination reactions as can be seen by comparing PES profiles given in Figures 3 and 4 and activation energies[41,42] for the thermal elimination reactions. In the reaction involving $i$-$C_3H_7Br$, perhaps one of the most striking effects derived from the $Na^+$ participation is the significant reduction in $\Delta_r H_0$ from 0.86 to 0.25 eV for reaction channel (1) and to 0.35 eV for reaction channel (2) as well as the lowering of the highest potential energy barrier TS1 in Figure 3 (0.166 eV) along the reaction process, while for the elimination reaction without sodium ion the potential energy barrier should be at least as high as the reaction's endothermicity (0.86 eV). A similar effect, even more pronounced, on the reaction energetics is found when $i$-$C_3H_7OH$ is considered, the dehydration reaction changing its endothermic character (0.86 eV) to an exothermic one, −0.036 eV for reaction channel (1) and −0.491 eV for reaction 2 as shown in Table 2 when the process is induced by collisions with sodium ions. Moreover, the potential energy profile along the $Na^+ + i$-$C_3H_7OH$ reaction evolution given in Figure 4 shows a relatively high potential energy barrier (TS1) that imposes a minimum energy requirement of ∼1.1 eV, notably lower that the transition states barrier (2.83 eV) calculated by quantum chemistry methods.[43] The activation energy for $i$-$C_3H_7OH$ dehydration when sodium ions are involved is reduced ∼2.6


DOI: 10.1021/acs.jpca.5b11869
J. Phys. Chem. A XXXX, XXX, XXX−XXX

times with respect to the gas-phase thermal elimination, according to data given in Table 2. Bearing in mind the considerations made on the effects of the participation of sodium ions in the dehydrohalogenation and dehydration reactions studied, it can be concluded in some way that the sodium ion plays the role of a catalyst for these elimination reactions.

## 5. CONCLUDING REMARKS

In this study, excitation functions in absolute units have been obtained for the different reactive process observed in the dehydrohalogenation and dehydration reactions of *i*-$C_3H_7Br$ and *i*-$C_3H_7OH$ gas-phase molecules in binary collisions with sodium ions using an octopole RF guide. In these reactions sodium ion appears either coordinated to the $C_3H_6$ double bond or to eliminated hydrogen bromide or water, as $[HBr-Na]^+$ or $[H_2O-Na]^+$ in reactions with *i*-$C_3H_7Br$ and *i*-$C_3H_7OH$, respectively. Moreover, the formation of an adduct between the sodium ion and the neutral molecule has been observed in a definite collision energy range for each reaction, as well as an additional decomposition reaction that appears at higher collision energies. The complementary quantum chemistry calculations done for both for $Na^+$ + *i*-$C_3H_7Br$ and $Na^+$ + *i*-$C_3H_7OH$ reactions give important information on the topology of the PESs on which reactive processes take place and help globally to interpret the shape of the measured excitation functions and, where present, the corresponding threshold energies being in good agreement with experimental results. Quantum chemistry ab initio calculations evidence that the interaction between $Na^+$ and *i*-$C_3H_7Br$ or *i*-$C_3H_7OH$ molecules is essentially noncovalent, the sodium atom conserving a high fraction of its original charge along reactive pathways and helping to promote the elimination in the corresponding molecule with the simultaneous formation of a carbon−carbon double bond. This effective role of the sodium ion on the atomic rearrangement along the reaction evolution as well as its effect on the reaction energetics and on the reaction potential energy barriers leads to conclude that sodium ions play the role of a catalyst in the gas-phase ion−molecule dehydrohalogenation and dehydration reactions studied.

## ■ AUTHOR INFORMATION

### Corresponding Author

*Fax: +34 93 402 12 31. E-mail: a.aguilar@ub.edu.

### Notes

The authors declare no competing financial interest.

## ■ ACKNOWLEDGMENTS

This work has been supported by the Spanish Ministerio de Economia y Competividad (MINECO Project CTQ2013-41307-P). Thanks are also due the Generalitat de Catalunya-AGAUR (Projects 2013 SGR 25) and to the Consorci de Serveis Universitaris de Catalunya (CSUC) and the Fundació Catalana per a la Recerca for allocating supercomputing time.

## ■ REFERENCES

(1) Sabidó, M.; Lucas, J. M.; de Andrés, J.; Sogas, J.; Albertí, M.; Aguilar, A.; Bassi, D.; Ascenzi, D.; Franceschi, P.; Tosi, P.; Pirani, F. Guided Ion Beams Study of Ion−Molecule Reactions at Low Collision Energies: The $Li^+$-Acetone Adduct Formation in the 0.10−1.00 eV Center of Mass Energy Range. *Chem. Phys. Lett.* **2007**, *442*, 28−34.

(2) Lucas, J. M.; de Andrés, J.; López, E.; Albertí, M.; Bofill, J. M.; Bassi, D.; Ascenzi, D.; Tosi, P.; Aguilar, A. Guided-Ion-Beam and Ab Initio Study of the $Li^+$, $K^+$ and $Rb^+$ Association Reactions with Gas Phase Butanone and Cyclohexanone in Their Ground Electronic States. *J. Phys. Chem. A* **2009**, *113*, 14766−14773.

(3) López, E.; Lucas, J. M.; de Andrés, J.; Albertí, M.; Bofill, J. M.; Bassi, D.; Aguilar, A. Cross-Section Energy Dependence of the $[C_6H_6-M]^+$ Adduct Formation Between Benzene Molecules and Alkali Ions (M= Li, Na, K). *Phys. Chem. Chem. Phys.* **2011**, *13*, 15977−15984.

(4) Rees, M. H. Chemical Ionic Reactions in the Thermosphere. In *Physics and Chemistry of the Upper Atmosphere;* Cambridge University Press: Cambridge, U.K., 1989; pp 278−281.

(5) De Andrés, J.; Lucas, J. M.; Albertí, M.; Bofill, J. M.; Aguilar, A. Study by Crossed Beams and Ab Initio Techniques of An Environmentally Interesting Process: Gas-Phase High Energy Collisions Between $N_2O(^1\Sigma^+)$ and $Li^+(^1S_0)$. *Chem. Phys.* **2015**, *462*, 104−110.

(6) McMahon, T. B.; Ohanessian, G. An Experimental and Ab Initio Study of the Nature of the Binding in Gas-Phase Complexes of Sodium Ions. *Chem. - Eur. J.* **2000**, *6*, 2931−2941.

(7) Klemperer, W.; Vaida, V. Molecular Complexes in Close and Far Away. *Proc. Natl. Acad. Sci. U. S. A.* **2006**, *103*, 10584−8.

(8) Wieting, R. D.; Staley, R. H.; Beauchamp, J. L. Reactions of Alkali Ions with Organic Molecules in the Gas Phase. Low Energy Pathways for Carbonium Ion Formation and Novel Methods for Generating Alkali Ion Complexes with.pi.- and n-Donor Bases. *J. Am. Chem. Soc.* **1975**, *97*, 924−926.

(9) Allison, J.; Ridge, D. P. Reactions of Transition Metal Ions with Alkyl Halides and Alcohols in the Gas Phase: Evidence for Metal Insertion and.beta.-Hydrogen Atom Shift. *J. Am. Chem. Soc.* **1976**, *98*, 7445−7447.

(10) Allison, J.; Ridge, D. P. Reactions of Atomic Metal Ions with Alkyl Halides and Alcohols in the Gas Phase. *J. Am. Chem. Soc.* **1979**, *101*, 4998−5009.

(11) Creasy, W. R.; Farrar, J. M. Intrinsic Barriers in Gas-Phase Dehydration Reactions: An Experimental Probe. *J. Phys. Chem.* **1985**, *89*, 3952−3955.

(12) Creasy, W. R.; Farrar, J. M. Reactive Scattering from Double Minimum Potentials: $Li^+$ Catalyzed Elimination Reactions of Alkali Halides. *J. Chem. Phys.* **1987**, *87*, 5280−5293.

(13) Lucas, J. M.; de Andrés, J.; Sogas, J.; Albertí, M.; Bofill, J. M.; Bassi, D.; Ascenzi, D.; Tosi, P.; Aguilar, A. An Experimental Guided-Ion-Beam and Ab Initio Study of the Ion−Molecule Gas Phase Reactions between $Li^+$ Ions and iso-$C_3H_7Cl$ in Their Ground Electronic State. *J. Chem. Phys.* **2009**, *131*, 024306(1).

(14) Lucas, J. M.; de Andrés, J.; Albertí, M.; Bofill, J. M.; Bassi, D.; Aguilar, A. Experimental Cross-Sections Energy Dependence and Ab Initio Electronic Structure Survey of the Ground Singlet Potential Surface for Reactive $Li^+$ + *n*-$ClC_3H_7$ Collisions at Low Energies. *Phys. Chem. Chem. Phys.* **2010**, *12*, 13646−13656.

(15) Aguilar, J.; Lucas, J. M.; de Andrés, J.; Albertí, M.; Bassi, D.; Aguilar, A. Reactive processes in Gas Phase $Na^+$-*iso*-$C_3H_7Cl$ Collisions: Experimental Guided-Ion-Beam and *Ab Initio* Studies of the Reactions on the Ground Singlet Potential Surface of the System up to 12.00 eV. *Phys. Chem. Chem. Phys.* **2011**, *13*, 18581−18591.

(16) Aguilar, J.; Lucas, J. M.; de Andrés, J.; Albertí, M.; Bassi, D.; Aguilar, A. Experimental Study of the Reactive Processes in the Gas Phase $K^+$ + *i*-$C_3H_7Cl$ Collisions. A Comparison with Li and Na Ions. *J. Chem. Phys.* **2013**, *138*, 184310.

(17) López, E.; Lucas, J. M.; de Andrés, J.; Albertí, M.; Bofill, J. M.; Bassi, D.; Aguilar, A. Experimental and Ab Initio Studies of the Reactive Processes in Gas Phase *i*-$C_3H_7Br$ and *i*-$C_3H_7OH$ Collisions with Potassium Ions. *J. Chem. Phys.* **2014**, *141*, 164310.

(18) Ervin, K. M.; Armentrout, P. B. Translational Energy Dependence of $Ar^+$ + $XY \rightarrow ArX^+$ + Y (XY = $H_2$, $D_2$, HD) from Thermal to 30 eV c.m. *J. Chem. Phys.* **1985**, *83*, 166−189.

(19) Chantry, P. J. *Doppler Broadening in Beam Experiments. J. Chem. Phys.* **1971**, *55*, 2746−2759.

(20) Lifshitz, C.; Wu, R. L. C.; Tiernan, T. O.; Terwilliger, D. T. Negative Ion−Molecule Reactions of Ozone and Their Implications on the Thermochemistry of $O_3^-$. *J. Chem. Phys.* **1978**, *68*, 247−259.



DOI: 10.1021/acs.jpca.5b11869
J. Phys. Chem. A XXXX, XXX, XXX−XXX

(21) Schlier, C. G. Cross Sections, Rate Constants, and Maxwellian Averages. *Chem. Phys.* **1988**, *126*, 73−80.
(22) Koizumi, H. P.; Armentrout, P. B. The Kinetic Energy Dependence of Association Reactions. A New Thermokinetic Method for Large Systems. *J. Chem. Phys.* **2003**, *119*, 12819−12829.
(23) Levine, R. D. *Molecular Reaction Dynamics;* Cambridge University Press, 2005; pp 4, 79, and References therein.
(24) Aikens, C. M.; Webb, S. P.; Bell, R. L.; Fletcher, G. D.; Schmidt, M. W.; Gordon, M. S. A Derivation of the Frozen-Orbital Unrestricted Open-Shell and Restricted Closed-Shell Perturbation Theory Analytic Gradient Expressions. *Theor. Chem. Acc.* **2003**, *110*, 233−253.
(25) Frisch, M. J.; Trucks, G. W.; Schlegel, H. B. et al. *Gaussian03,* Revision E.01; Gaussian Inc: Wallingford, CT, 2004.
(26) Gordon, M. S.; Schmidt, M. W.; Dykstra, C. E.; Frenking, G.; Kim, K. S.; Scuseria, G. E. *Theory and Applications of Computational Chemistry*: The First Forty Years; Elsevier, 2005; p 1167.
(27) Fukui, K. Formulation of the Reaction Coordinate. *J. Phys. Chem.* **1970**, *74*, 4161−4163.
(28) Gonzalez, C.; Schlegel, H. B. An Improved Algorithm for Reaction Path Following. *J. Chem. Phys.* **1989**, *90*, 2154−2161.
(29) http://webbook.nist.gov/chemisty/.
(30) Baer, T. Gas-Phase Heats of Formation of $C_2H_5^+$ and $C_3H_7^+$. *J. Am. Chem. Soc.* **1980**, *102*, 2482−2483.
(31) *CRC Handbook of Chemistry and Physics,* 77th ed.; Lide, D. R., Ed.; CRC Press: Boca Raton, 1996; pp 5−34 and 9−37.
(32) Cioslowski, J. A New Population Analysis Based on Atomic Polar Tensors. *J. Am. Chem. Soc.* **1989**, *111*, 8333−8336.
(33) López, E.; Lucas, J. M.; de Andrés, J.; Albertí, M.; Bofill, J. M.; Bassi, D.; Aguilar, A. Cross-Section Energy Dependence of the $[C_6H_6$-M$]^+$ Adduct Formation Between Benzene Molecules and Alkali Ions (M= Li, Na, K). *Phys. Chem. Chem. Phys.* **2011**, *13*, 15977−15984.
(34) Lucas, J. M.; De Andrés, J.; Albertí, M.; Bofill, J. M.; Aguilar-Navarro, A. An *Ab Initio* Theoretical Study Approach to the Gas Phase Decomposition of $C_3H_7^+$ Produced in Ground State $Li^+$ + *iso*-$ClC_3H_7$ Collisions. *Int. J. Quantum Chem.* **2011**, *111*, 493−504.
(35) http://cccbdb.nist.gov/.
(36) Aguilar, J.; de Andrés, J.; Lucas, J. M.; Albertí, M.; Huarte-Larrañaga, F.; Bassi, D.; Aguilar, A. Dynamics of Alkali Ions-Neutral Molecules Reactions: Radio Frequency-Guided Beam Experimental Cross-Sections and Direct Quasiclassical Trajectory Studies. *AIP Conf. Proc.* **2012**, *1501*, 1340−1349.
(37) Aguilar, A.; Gilibert, M.; Giménez, X.; González, M.; Sayós, R. Dynamics of the $N(^4S)$ + $NO(X\ ^2\Pi)$ → $N_2(X\ ^1\Sigma_g^+)$ + $O(^3P)$ Atmospheric Reaction on the 3A" Ground Potential Energy Surface. III. Quantum Dynamical Study and Comparison with Quasiclassical and Experimental Results. *J. Chem. Phys.* **1995**, *103*, 4496−4508.
(38) Batey, J. H.; Tedder, J. M. The Study of Ion−Molecule Reactions in the Gas Phase Using a Triple Quadrupole Mass Spectrometer. Part 1. The Reactions of $CH_3^+$, $CD_3^+$, and $C_2H_5^+$ with Simple Olefins. *J. Chem. Soc., Perkin Trans. 2* **1983**, 1263−1267.
(39) Lucas, J. M.; De Andrés, J.; Albertí, M.; Bofill, J. M.; Aguilar-Navarro, A. An Ab Initio Theoretical Study Approach to the Gas Phase Decomposition of $C_3H_7^+$ Produced in Ground State $Li^+$ + *iso*-$ClC_3H_7$ Collisions. *Int. J. Quantum Chem.* **2011**, *111*, 493−504.
(40) Benson, S. W. *The Foundations of Chemical Kinetics;* McGraw Hill Book Company: New York, 1960; pp 319−424.
(41) Benson, S. W.; O'Neal, H. E. *Kinetic Data on Gas Phase Unimolecular Reactions,* National Bureau of Standards, United States Department of Commerce, 1970; p 95.
(42) Frassoldati, A.; Cuoci, A.; Faravelli, T.; Niemann, U.; Ranzi, E.; Seiser, R.; Seshadri, K. An Experimental and Kinetic Modeling Study of *n*-Propanol and *iso*-Propanol Combustion. *Combust. Flame* **2010**, *157*, 2−16.
(43) Bui, B. H.; Zhu, R. S.; Lin, M. C. Thermal Decomposition of iso-Propanol: First-Principles Prediction of Total and Product-Branching Rate Constants. *J. Chem. Phys.* **2002**, *117*, 11188−11195.


DOI: 10.1021/acs.jpca.5b11869
*J. Phys. Chem. A* XXXX, XXX, XXX−XXX